AGU PUBLICATIONS

Geophysical Research Letters

RESEARCH LETTER
10.1002/2015GL066928

Key Points:
- Initialization differences in sea ice area are amplified during summer and dampened during winter
- Uncertain spring sea ice coverage causes significantly different Arctic summer temperature forecasts
- Skill of European and North American temperature forecasts depends on sea ice satellite product

Supporting Information:
- Supporting Information S1

Correspondence to:
F. Bunzel,
felix.bunzel@mpimet.mpg.de

Citation:
Bunzel, F., D. Notz, J. Baehr, W. A. Müller, and K. Fröhlich (2016), Seasonal climate forecasts significantly affected by observational uncertainty of Arctic sea ice concentration, *Geophys. Res. Lett.*, *43*, 852–859, doi:10.1002/2015GL066928.

Received 6 NOV 2015
Accepted 7 JAN 2016
Accepted article online 12 JAN 2016
Published online 29 JAN 2016

Seasonal climate forecasts significantly affected by observational uncertainty of Arctic sea ice concentration

Felix Bunzel[1], Dirk Notz[1], Johanna Baehr[2], Wolfgang A. Müller[1], and Kristina Fröhlich[3]

[1]Ocean in the Earth System, Max Planck Institute for Meteorology, Hamburg, Germany, [2]Institute of Oceanography, Center for Earth System Research and Sustainability, Universität Hamburg, Hamburg, Germany, [3]Deutscher Wetterdienst, Offenbach, Germany

Abstract We investigate how observational uncertainty in satellite-retrieved sea ice concentrations affects seasonal climate predictions. To do so, we initialize hindcast simulations with the Max Planck Institute Earth System Model every 1 May and 1 November from 1981 to 2011 with two different sea ice concentration data sets, one based on the NASA Team and one on the Bootstrap algorithm. For hindcasts started in November, initial differences in Arctic sea ice area and surface temperature decrease rapidly throughout the freezing period. For hindcasts started in May, initial differences in sea ice area increase over time. By the end of the melting period, this causes significant differences in 2 meter air temperature of regionally more than 3°C. Hindcast skill for surface temperatures over Europe and North America is higher with Bootstrap initialization during summer and with NASA Team initialization during winter. This implies that the observational uncertainty also affects forecasts of teleconnections that depend on northern hemispheric climate indices.

1. Introduction

The observed rapid decrease in Arctic sea ice area over the past few decades [*Stroeve et al.*, 2012] might affect weather patterns in midlatitudes [*Francis and Vavrus*, 2012]. This is one reason why seasonal climate forecasts increasingly account for the role of sea ice by including sea ice concentration into the data assimilation process [e.g., *Sigmond et al.*, 2013; *Wang et al.*, 2013; *Peterson et al.*, 2015]. Initializing sea ice thickness was also found to improve the seasonal prediction skill of Arctic sea ice area in potential predictability studies [e.g., *Chevallier and Salas-Mélia*, 2012; *Day et al.*, 2014]; however, consistent pan-Arctic observational time series exceeding a few years are still lacking. For initialization of sea ice concentrations, different data products were used in recent studies. For example, *Sigmond et al.* [2013] assimilated Hadley Centre Sea Ice and Sea Surface Temperature ice concentrations [*Rayner et al.*, 2003], which is a combined analysis product based on a variety of data sources, while *Wang et al.* [2013] assimilated sea ice data from passive microwave retrievals, such as the NASA Team ice concentration time series [*Cavalieri*, 1994; *Cavalieri et al.*, 1996]. However, retrieval algorithms deriving sea ice concentrations from the same satellite passive microwave data record differ in their resulting Arctic sea ice area by up to 1.3 million km^2 [*Ivanova et al.*, 2014]. Here we show that these differences significantly affect seasonal predictions, which we exemplify for Arctic sea ice area and 2 meter air temperature. We assimilate the NASA Team [*Cavalieri et al.*, 1996] and the Bootstrap [*Comiso*, 2000] sea ice concentration data sets into the Max Planck Institute Earth System Model (MPI-ESM) [*Stevens et al.*, 2013]. Both data sets were compiled at the National Snow and Ice Data Center (NSIDC) and were derived from the same satellite record of brightness temperatures. The only difference between the two products is the algorithm used to derive sea ice concentrations from the original satellite record. From each of the two assimilation runs a set of seasonal hindcast experiments is started. Thus, the impact of the assimilated sea ice concentration data product on hindcast skill in our MPI-ESM seasonal prediction system can be assessed.

The detailed experimental setup is given in section 2 together with a brief description of the seasonal prediction system. The impact of the assimilated sea ice product on the prediction of Arctic sea ice area and 2 meter air temperature is evaluated in sections 3 and 4, respectively, while conclusions are drawn in section 5.

2. Model Description and Experimental Setup

All experiments in this study are conducted using the seasonal prediction system described in detail by *Baehr et al.* [2015]. This system is based on the Max Planck Institute Earth System Model (MPI-ESM), which is one of the models that contributed to the Coupled Model Intercomparison Project 5 [*Taylor et al.*, 2012]. We use the low-resolution (LR) configuration, where the atmosphere component of MPI-ESM, ECHAM6 [*Stevens et al.*, 2013], has a horizontal resolution of T63 ($\approx 1.9°\times1.9°$) and 47 levels between the surface and 0.01 hPa. The ocean component is the Max Planck Institute Ocean Model (MPIOM) [*Jungclaus et al.*, 2013], which in the LR setup has a nominal resolution of 1.5° with two poles located in South Greenland and in Antarctica. This translates to a horizontal resolution of 15 km in the vicinity of Greenland and 185 km in the tropical Pacific. In the vertical, the ocean is resolved with 40 levels, with a distance between the centers of two levels ranging from 10 to 250 m. The sea ice component within MPIOM consists of a dynamic/thermodynamic sea ice model based on *Hibler* [1979]. The mean state and variability of Arctic sea ice is realistically simulated in MPI-ESM, as evaluated by *Notz et al.* [2013]. The effect of melt ponds is indirectly accounted for by a melt pond parameterization that affects surface albedo [*Roeckner et al.*, 2012].

For this study, two assimilation experiments are performed with MPI-ESM-LR, differing only in the assimilated sea ice concentration data product, which is a gridded product with 25×25 km resolution of either the NASA Team (hereafter NT) [*Cavalieri et al.*, 1996] or the Bootstrap (hereafter BT) [*Comiso*, 2000] sea ice concentration retrieval. Both data products are interpolated bilinearly to the model grid before assimilation. In grid boxes containing missing values, e.g., the polar observation hole, no assimilation is applied, meaning that the sea ice is here exclusively calculated by the model. Since sea ice concentration retrieval algorithms commonly use satellite brightness temperatures to derive ice concentrations and since melt ponds are not distinguishable from open water in terms of their brightness temperature, melt ponds are per se retrieved as open water by both algorithms. To partly account for this bias in retrieved sea ice concentration, the BT algorithm synthetically increases the ice concentration during summer. This procedure reduces biases in some areas but may introduce a positive bias in sea ice concentration in regions without melt ponds. In the NT data set, no such bias correction is applied.

The two assimilation experiments cover the period 1979–2012. Newtonian relaxation (or "nudging") is used as assimilation technique, and besides sea ice concentration, also observations of atmospheric and oceanic quantities are nudged into the model using full-field data assimilation in all atmospheric and oceanic levels. In the atmosphere, vorticity, divergence, temperature, and surface pressure are nudged into the model with a relaxation time of 1 day, while salinity and temperature in the ocean are nudged with a relaxation time of 10 days. For assimilation of atmospheric quantities, the European Centre for Medium-Range Weather Forecasts Reanalyses ERA-Interim [*Dee et al.*, 2011] is used, the ocean is nudged toward Ocean Reanalysis System 4 data [*Balmaseda et al.*, 2013]. For assimilation of NT and BT sea ice concentrations a relaxation time of 20 days is used. Relaxation times differ among the model components in order to account for the different response times of the components. In order to allow for a realistic relation between ice concentration and thickness, sea ice thickness is updated in the model proportionally to ice concentration nudging [*Tietsche et al.*, 2013]. This causes by definition ice thickness differences which are well related to differences in assimilated sea ice concentration data sets.

From each of the two assimilation experiments a 10-member ensemble of 6-month hindcast simulations is started every year on 1 May and 1 November. Ensemble members are generated by small disturbances of both oceanic and atmospheric states. In the ocean, "breeding" is used to add a small disturbance to the global three-dimensional ocean temperature and salinity fields [*Baehr and Piontek*, 2013], while in the atmosphere the stratospheric diffusion is slightly varied among the ensemble members.

3. Impact on Predicted Arctic Sea Ice Area

Due to the different characteristics of NT and BT sea ice concentration data sets, the Arctic sea ice area derived from the BT product is substantially larger than that for the NT product. The absolute ice area surplus in the BT product ranges from 0.5 million km^2 in May to 1.2 million km^2 during the Arctic melting season (Figure 1, solid black line), with the maximum surplus occurring during the melt pond maximum in July. This characteristic is well represented by the assimilation experiments with MPI-ESM (Figure 1, dashed black line).

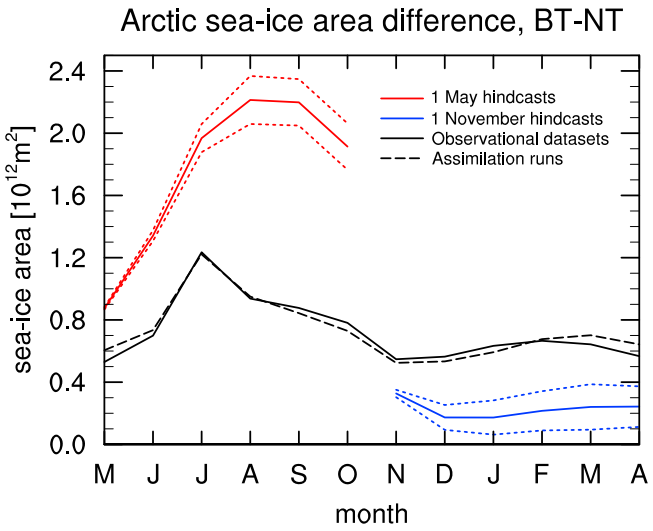

Figure 1. Differences in monthly mean Arctic sea ice area between Bootstrap (BT) and NASA Team (NT) data products, as derived from the original data products (solid line), the corresponding assimilation experiments (dashed line), as well as the 1 May (red) and 1 November (blue) hindcast experiments are shown. Dotted lines (red and blue) indicate ±2 sigma intervals for ensemble means of hindcast experiments.

When hindcast ensemble simulations are started during the Arctic melting period, the initial difference in sea ice area increases over time (Figure 1, red line), which indicates that the evolution of sea ice area is controlled by positive feedbacks throughout summer, of which the ice-albedo feedback is most important. As a consequence, comparing anomaly correlations obtained for the two hindcast sets shows that the hindcast skill for Arctic sea ice area strongly depends on the sea ice data product used for model initialization during summer: Initialization with NT sea ice concentrations outperforms initialization with BT sea ice in all hindcast months except for July, where BT initialization yields better skill (Figure 2, top). In this month the spread of NT hindcasts is almost 50% larger compared to BT hindcasts, resulting in a large spread-error ratio and, thus, a decrease in reliability of NT compared to BT hindcasts.

When hindcasts are initialized during the Arctic freezing period, initial differences in sea ice area reduce then stabilize (Figure 1, blue line). This shows that negative feedbacks control the evolution of sea ice during the freezing period, most importantly the loss of long-wave radiation that causes a rapid formation of thin layers of sea ice in regions with sea surface temperatures close to the freezing point. Correspondingly, the hindcast skill for Arctic sea ice area barely depends on the sea ice data product used for model initialization on 1 November (Figure 2, bottom).

Independent of the product used for initialization, we find that anomaly correlations of predicted sea ice area during the Arctic melting period are substantially larger if the BT sea ice product is used as reference data set, even if the model is initialized with NT sea ice (Figure 2, top). This implies that during the summer melt period, the evolution of Arctic sea ice in MPI-ESM corresponds better with BT than with NT sea ice. This can possibly be explained by the fact that the BT algorithm partly compensates for the well-known negative biases in retrieved sea ice concentration that are caused by surface melt ponds.

A regional evaluation of the differences between the two hindcast sets shows that for initialization on 1 May there is a small initial surplus of sea ice in BT hindcasts in the Hudson Bay, Davis Strait, and Greenland Sea, while in September differences become significant over almost the entire Arctic Ocean (Figures 3a and 3b). Since, for instance, anomalies in the summer sea ice extent over the Barents, Kara, and Laptev Seas were found to be connected to certain prevailing sea level pressure anomaly patterns [*Deser et al.*, 2000], the difference in sea ice concentrations in these regions may impact teleconnections with northern hemispheric climate indices.

For initialization on 1 November differences in sea ice area between the two hindcast sets are generally small. Until the end of the freezing period a significant surplus of sea ice in BT hindcasts builds up in the Denmark Strait and Greenland Sea (Figures 3c and 3d). However, in some regions where the initial difference was close to zero, e.g., in the central Arctic, the ensemble mean of NT hindcasts slightly exceeds the sea ice concentration in the ensemble mean of BT hindcasts.

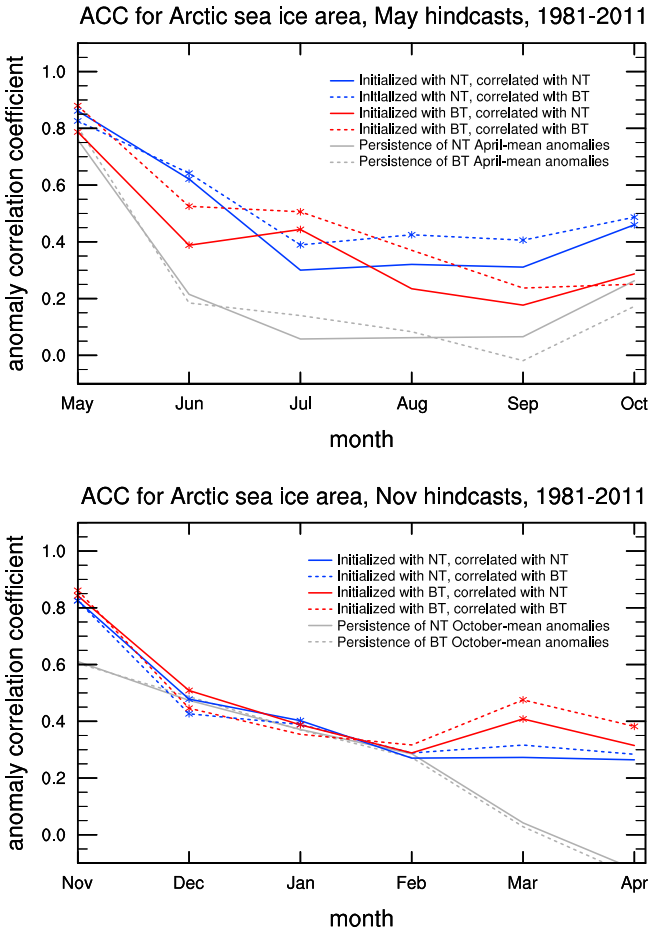

Figure 2. The anomaly correlation coefficient (ACC) between observed and predicted Arctic sea ice area is shown. Climatology and linear trend were removed from original fields to obtain anomalies. Predicted sea ice area was derived from hindcast simulations with MPI-ESM started on (top) 1 May and (bottom) 1 November. One set of hindcasts was initialized with NT sea ice data (blue), another set was initialized with BT data (red). Predicted sea ice area anomalies were correlated with observed NT (solid lines) and BT (dotted lines) anomalies. The persistence of observed April and October anomalies is shown for reference (grey). Stars indicate significant ACCs at the 95% level obtained from a distribution of 1000 resampled 10 member ensemble means [*Goddard et al.*, 2013].

These differences in sea ice concentration obviously cause differences in 2 m air temperatures. These we turn to now.

4. Impact on Predicted Arctic 2 Meter Air Temperature

During the melting period, melt water covering the ice surface forces Arctic air temperatures toward the freezing point of water. Thus, the impact of differences in sea ice initialization on Arctic 2 meter air temperatures remains small as long as Arctic melting is in progress (Figure 3e). At the end of the melting period, however, air temperature drops much more rapidly over ice than over open water, causing the surplus in sea ice area in hindcasts initialized with the BT sea ice product to manifest in significantly colder surface air temperatures once the ice surface ceases to melt (Figure 3f). These differences in surface temperatures are particularly prominent in the vicinity of the ice edge, where the pattern agrees well with differences in sea ice concentrations (Figure 3b). However, surface temperature differences extend farther south than ice concentration differences, which is because of the integrated effect of the sea ice retreating earlier in NT compared to BT hindcasts in the months before September.

The impact of the sea ice product used for model initialization on the mean hindcast error of September 2 meter air temperatures varies regionally. Compared to an initialization with NT, a BT-based initialization reduces the hindcast error by up to 30% over the East Siberian Sea but increases the mean hindcast error by

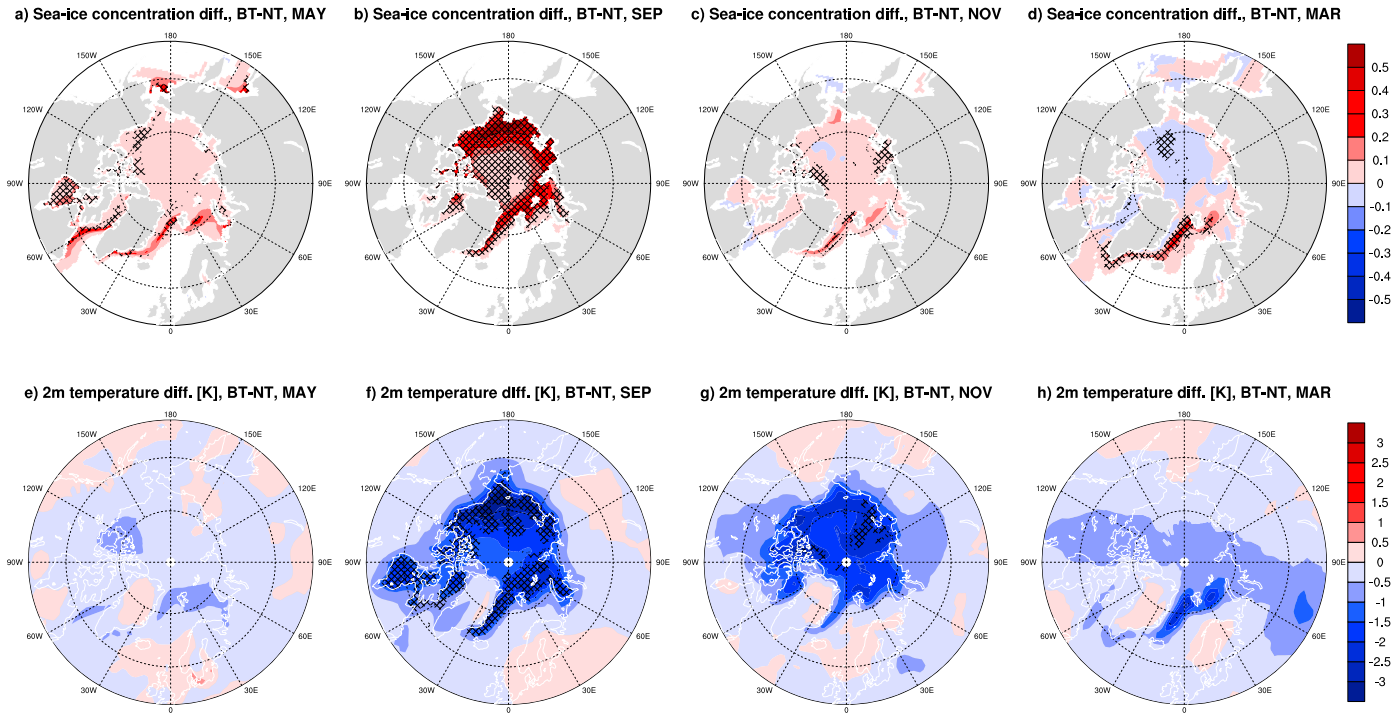

Figure 3. (a–d) The difference in monthly mean sea ice concentration and (e–h) 2 meter air temperature between the ensemble mean of BT and NT hindcast sets that started on 1 May is shown for May (Figures 3a and 3e) and September (Figures 3b and 3f). The same difference is also shown for hindcast sets started on 1 November (Figures 3c, 3d, 3g, and 3h). The black lattice pattern indicates significant differences at the 95% level after a Kolmogorov-Smirnov test.

up to 30% over the Laptev Sea and Barents Sea (Figure 4, top). Over the North American and European continents initialization with BT sea ice yields hindcast errors which are 20% lower and also shows larger anomaly correlations for September 2 meter air temperatures (supporting information Figure S1, top) compared to initialization with NT sea ice.

When the two hindcast sets are initialized during the Arctic freezing period, the 2 meter temperature difference, originating also in the assimilation experiments from sea ice area differences at the end of the melting period, still prevails over large regions (Figure 3g). At the end of the Arctic freezing period, however, except for a small area in the Greenland Sea where also ice concentrations differ significantly (Figure 3d), 2 meter air temperatures are not significantly different between the two hindcast sets anymore (Figure 3h). During Arctic freezing, differences in near-surface air temperatures reduce over time, as differences in Arctic sea ice area decrease because of the dominating role of negative feedbacks as discussed above (Figure 1).

The sea ice product used for model initialization also impacts the seasonal mean hindcast error of December-January-February (DJF) mean 2 meter air temperatures. Over Eastern Europe and Eurasia initialization with NT sea ice yields 10–20% lower hindcast errors compared to initialization with BT sea ice (Figure 4, bottom). Over the Greenland Sea the mean hindcast error is even reduced by up to 30% when NT sea ice initialization is used, which may be due to positive ice concentration biases induced by the ad hoc bias correction applied in the BT data product. Also, anomaly correlations for DJF mean 2 meter air temperature are significantly larger in these regions for NT compared to BT initialization (supporting information Figure S1, bottom). Over Northeast Canada and the North Pacific, on the other hand, BT initialization yields significantly lower hindcast errors than NT initialization. Thus, the sea ice concentration data set used to initialize seasonal hindcasts does not only affect sea ice area but also near-surface air temperature predictions, which may yield implications for teleconnections with northern hemispheric climate indices. However, sea level pressure and 500 hPa geopotential height are in this experimental setup not significantly different between the two hindcast sets.

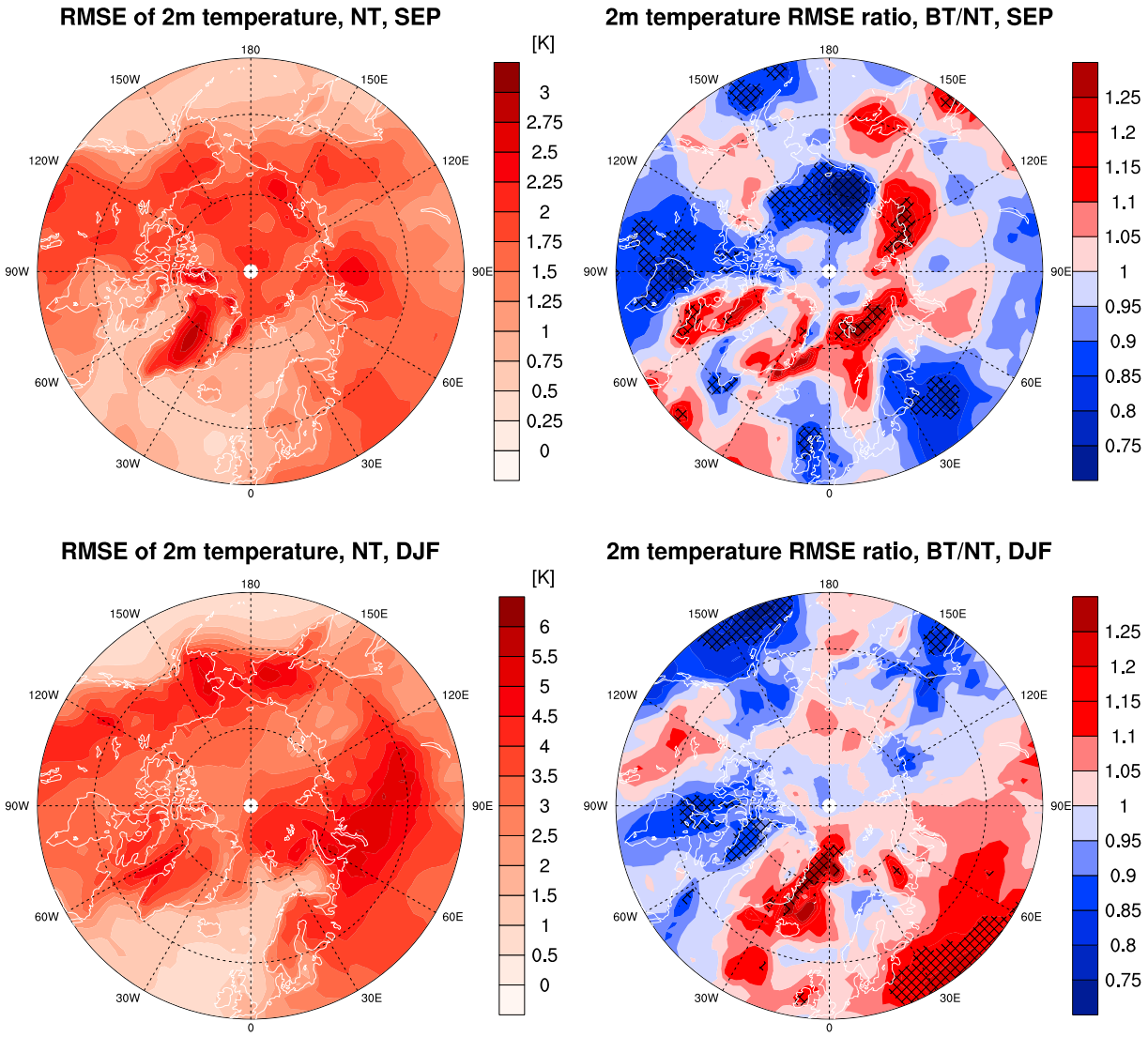

Figure 4. The root-mean-square error (RMSE) between predicted 2 meter temperature and ERA-Interim reanalyses is shown. The climatology of the respective data set was removed from original fields before computation of RMSEs. (top) RMSEs are presented for September (hindcasts started on 1 May) and (bottom) DJF (hindcasts started on 1 November) 2 meter temperature derived from hindcasts initialized with NT sea ice (left). The RMSE ratio of BT/NT initializations (right) is also shown. The black lattice pattern indicates significant differences at the 95% level obtained from a distribution of 1000 resampled 10 member ensemble means [*Goddard et al.*, 2013].

5. Summary and Conclusions

Since the potential to significantly increase the seasonal prediction skill of the Arctic sea ice cover by initializing sea ice concentration data was recognized, several studies have been carried out using different ice concentration products for model initialization [e.g., *Sigmond et al.*, 2013; *Wang et al.*, 2013; *Peterson et al.*, 2015]. In our systematic comparison of two hindcast sets differing only in the assimilated sea ice concentration data set, we assess the impact of the assimilated sea ice product on seasonal prediction focussing on Arctic sea ice area and 2 meter air temperature. The predicted Arctic sea ice area strongly depends on the assimilated sea ice product when the hindcast is started during the Arctic melting season. This is because during summer, positive feedbacks amplify initial differences in Arctic sea ice area over time. The growing differences in simulated sea ice area go along with significant differences in near-surface air temperatures, reaching at the end of the melting period regionally more than 3°C. When the hindcast is started during the Arctic freezing period, negative feedbacks dominate and initial differences in sea ice area and near-surface air temperature decrease over time. As a consequence, at the end of the freezing period the two hindcast sets are in most regions not significantly distinguishable anymore. This is because any surplus in oceanic heat content that builds up in

the Arctic during the melting period is rapidly returned to the atmosphere at the beginning of Arctic freezing and then leaves the atmosphere through increased long-wave emission and reduced atmospheric heat advection from lower latitudes [*Tietsche et al.*, 2011].

The present study also emphasizes the importance of accounting for the characteristics of a sea ice concentration data set used for assimilation into a climate model. When ice concentration products, which per se do not distinguish between melt ponds and open water, are assimilated into an ocean model, large amounts of sea ice beneath melt ponds may be lost in the assimilation process during the Arctic melting period. To address this issue, in the BT data set the ice concentration is synthetically increased during summer. This results in a better correspondence between the sea ice product and model physics for BT compared to NT data in terms of the sea ice area anomaly during the Arctic melting period. Furthermore, BT sea ice initialization in May gives better hindcast skill for September near-surface air temperatures over North America and Europe compared to NT sea ice initialization.

Also, the hindcast skill for DJF 2 meter air temperature is found to depend on the sea ice data set used to initialize seasonal hindcasts. Here the NT data set gives 10–20% lower mean hindcast errors over Eastern Europe and Eurasia and up to 30% lower errors than the BT data set over the Greenland Sea. Since many northern hemispheric climate variability modes, such as the Arctic Oscillation [*Thompson and Wallace*, 1998], are based on DJF surface climate conditions, the potential impact of biases in the assimilated sea ice concentration data set on the seasonal prediction of key climate indices and their teleconnections in the Northern Hemisphere should be investigated in further studies.

In summary, different characteristics of sea ice concentration data products are shown to affect not only seasonal predictions of Arctic sea ice area but also result in significantly different near-surface air temperatures over large areas. This indicates that there is potential to improve model predictions by better accounting for the characteristics of the sea ice data set assimilated into a specific climate model.

Acknowledgments
This research is funded by the European Union's Seventh Framework Programme (FP7/20072013) under grant agreement 308378 ENV.2012.6.1-1, Seasonal-to-decadal Prediction for the Advancement of European Climate Services (http://www.specs-fp7.eu), and by the European Space Agency (ESA) through the project Sea Ice Climate Change Initiative (SICCI, http://esa-cci.nersc.no). The authors thank the National Snow and Ice Data Center (NSIDC) for providing Bootstrap and NASA Team sea ice concentration data products. Primary data and scripts used in the analysis and other supporting information that may be useful in reproducing the author's work are archived by the Max Planck Institute for Meteorology and can be obtained by contacting publications@mpimet.mpg.de.

References

Baehr, J., and R. Piontek (2013), Ensemble initialization of the oceanic component of a coupled model through bred vectors at seasonal-to-interannual time scales, *Geosci. Model Dev.*, *7*, 453–461.

Baehr, J., K. Fröhlich, M. Botzet, D. Domeisen, L. Kornblueh, D. Notz, R. Piontek, H. Pohlmann, S. Tietsche, and W. A. Mueller (2015), The prediction of surface temperature in the new seasonal prediction system based on the MPI-ESM coupled climate model, *Clim. Dyn.*, *44*(9–10), 2723–2735.

Balmaseda, M. A., K. Mogensen, and A. T. Weaver (2013), Evaluation of the ECMWF ocean reanalysis system ORA-S4, *Q. J. R. Meteorol. Soc.*, *139*(674), 1132–1161.

Cavalieri, D. J. (1994), Sea ice algorithm in NASA sea ice validation program for the defense meteorological satellite program special sensor microwave imager: Final Rep., NASA Tech. Memo. 104559, pp. 25–32, NASA Goddard Space Flight Cent., Greenbelt, Md.

Cavalieri, D. J., C. Parkinson, P. Gloersen, and H. J. Zwally (1996), Sea ice concentrations from Nimbus-7 SMMR and DMSP SSM/I-SSMIS passive microwave data, version 1. NASA Natl. Snow and Ice Data Cent. Distrib. Act. Arch. Cent., Boulder, Colo. [Available at: http://dx.doi.org/10.5067/8GQ8LZQVL0VL], accessed on 04/08/2014, updated yearly.

Chevallier, M., and D. Salas-Mélia (2012), The role of sea ice thickness distribution in the Arctic sea ice potential predictability: A diagnostic approach with a coupled GCM, *J. Clim.*, *25*(8), 3025–3038.

Comiso, J. C. (2000), Bootstrap sea ice concentrations from Nimbus-7 SMMR and DMSP SSM/I-SSMIS, version 2. NASA Natl. Snow and Ice Data Cent. Distrib. Act. Arch. Cent., Boulder, Colo. [Available at: http://dx.doi.org/10.5067/J6JQLS9EJ5HU], Data downloaded on 04/08/2014, updated 2015.

Day, J. J., E. Hawkins, and S. Tietsche (2014), Will Arctic sea ice thickness initialization improve seasonal forecast skill?, *Geophys. Res. Lett.*, *41*, 7566–7575, doi:10.1002/2014GL061694.

Dee, D., et al. (2011), The ERA-Interim reanalysis: Configuration and performance of the data assimilation system, *Q. J. R. Meteorol. Soc.*, *137*(656), 553–597.

Deser, C., J. E. Walsh, and M. S. Timlin (2000), Arctic sea ice variability in the context of recent atmospheric circulation trends, *J. CLim.*, *13*(3), 617–633.

Francis, J. A., and S. J. Vavrus (2012), Evidence linking Arctic amplification to extreme weather in mid-latitudes, *Geophys. Res. Lett.*, *39*, L06801, doi:10.1029/2012GL051000.

Goddard, L., et al. (2013), A verification framework for interannual-to-decadal predictions experiments, *Clim. Dyn.*, *40*(1–2), 245–272.

Hibler, W. (1979), A dynamic thermodynamic sea ice model, *J. Phys. Oceanogr.*, *9*(4), 815–846.

Ivanova, N., O. M. Johannessen, L. T. Pedersen, and R. T. Tonboe (2014), Retrieval of Arctic sea ice parameters by satellite passive microwave sensors: A comparison of eleven sea ice concentration algorithms, *IEEE Trans. Geosci. Remote Sens.*, *52*(11), 7233–7246.

Jungclaus, J., N. Fischer, H. Haak, K. Lohmann, J. Marotzke, D. Matei, U. Mikolajewicz, D. Notz, and J. Storch (2013), Characteristics of the ocean simulations in the Max Planck Institute Ocean Model (MPIOM) the ocean component of the MPI-Earth system model, *J. Adv. Model. Earth Syst.*, *5*, 422–446, doi:10.1002/jame.20023.

Notz, D., F. A. Haumann, H. Haak, J. H. Jungclaus, and J. Marotzke (2013), Arctic sea-ice evolution as modeled by Max Planck Institute for Meteorology's Earth system model, *J. Adv. Model. Earth Syst.*, *5*, 173–194, doi:10.1002/jame.20016.

Peterson, K. A., A. Arribas, H. Hewitt, A. Keen, D. Lea, and A. McLaren (2015), Assessing the forecast skill of Arctic sea ice extent in the GloSea4 seasonal prediction system, *Clim. Dyn.*, *44*(1–2), 147–162.

Rayner, N., D. E. Parker, E. Horton, C. Folland, L. Alexander, D. Rowell, E. Kent, and A. Kaplan (2003), Global analyses of sea surface temperature, sea ice, and night marine air temperature since the late nineteenth century, *J. Geophys. Res.*, *108*(D14), 4407, doi:10.1029/2002JD002670.

Roeckner, E., T. Mauritsen, M. Esch, and R. Brokopf (2012), Impact of melt ponds on Arctic sea ice in past and future climates as simulated by MPI-ESM, *J. Adv. Model. Earth Syst.*, *4*, M00A02, doi:10.1029/2012MS000157.

Sigmond, M., J. Fyfe, G. Flato, V. Kharin, and W. Merryfield (2013), Seasonal forecast skill of Arctic sea ice area in a dynamical forecast system, *Geophys. Res. Lett.*, *40*, 529–534, doi:10.1002/grl.50129.

Stevens, B., et al. (2013), Atmospheric component of the MPI-M Earth System Model: ECHAM6, *J. Adv. Model. Earth Syst.*, *5*, 146–172, doi:10.1002/jame.20015.

Stroeve, J. C., M. C. Serreze, M. M. Holland, J. E. Kay, J. Malanik, and A. P. Barrett (2012), The Arctic's rapidly shrinking sea ice cover: A research synthesis, *Clim. Change*, *110*(3–4), 1005–1027.

Taylor, K. E., R. J. Stouffer, and G. A. Meehl (2012), An overview of CMIP5 and the experiment design, *Bull. Am. Meteorol. Soc.*, *93*(4), 485–498.

Thompson, D. W., and J. M. Wallace (1998), The Arctic oscillation signature in the wintertime geopotential height and temperature fields, *Geophys. Res. Lett.*, *25*(9), 1297–1300.

Tietsche, S., D. Notz, J. Jungclaus, and J. Marotzke (2011), Recovery mechanisms of Arctic summer sea ice, *Geophys. Res. Lett.*, *38*, L02707, doi:10.1029/2010GL045698.

Tietsche, S., D. Notz, J. Jungclaus, and J. Marotzke (2013), Assimilation of sea-ice concentration in a global climate model–physical and statistical aspects, *Ocean Sci.*, *9*, 19–36.

Wang, W., M. Chen, and A. Kumar (2013), Seasonal prediction of Arctic sea ice extent from a coupled dynamical forecast system, *Mon. Weather Rev.*, *141*(4), 1375–1394.